International Journal of Engineering Science 169 (2021) 103563

Contents lists available at ScienceDirect

International Journal of Engineering Science

journal homepage: www.elsevier.com/locate/ijengsci

Numerical and experimental studies of acoustic streaming effects on microparticles/droplets in microchannel flow

Sadaf Maramizonouz [a], Mohammad Rahmati [a,*], Andreas Link [b], Thomas Franke [b], Yongqing Fu [a]

[a] Faculty of Engineering and Environment, Northumbria University, Newcastle upon Tyne, NE1 8ST, UK
[b] Division of Biomedical Engineering, James Watt School of Engineering, University of Glasgow, Glasgow, G12 8LT, UK

ARTICLE INFO

Keywords:
Acoustofluidics
Acoustic streaming
Numerical simulation
Particle deflecting
Particle directing
Microfluidic flow simulation

ABSTRACT

Exploiting acoustic streaming effects for microfluidic devices has been proven to be important for cell, microparticle and fluid manipulation in many fields such as, biomedical engineering, medical diagnostic devices, cell studies and chemistry. Acoustic streaming is used in acoustofluidic systems for directing and sorting microparticles as well as mixing and pumping fluids. To understand the underlying physics of such acoustofluidic systems and thus use them more efficiently in practical setups, computational modelling is critically needed. Although some work has been done to numerically model acoustofluidic systems, there are few studies to evaluate the capability and accuracy of different numerical schemes for analysing this complex multi-physics problem and to be directly validated by experiments. This paper aims to investigate the acoustic streaming effects caused by surface acoustic waves in a microchannel flow by using two different computational approaches to model the acoustic effects in three dimensions. In the first approach, we model the whole acoustic field caused by the oscillating lower wall. Here, the acoustic streaming effects were directly calculated from the density and velocity fields caused by the acoustic field. In the second approach, a low fidelity model is employed to capture the effects of acoustic streaming without modelling the acoustic field itself. In this approach, we substituted the velocity of a one-dimensional attenuating wave in the acoustic streaming force formula, and calculated the acoustic streaming force without using the density and velocity caused by the acoustic field. Both the computational methods are then validated by the results obtained from microflow experiments. The results from the second approach are in reasonable agreement with experiments while being more efficient in terms of computational cost. On the contrary, the first approach, while being computationally more expensive, allows to estimate the pressure field resulting from acoustic waves and thus predicts the dynamic behaviour of microparticles more accurately. Results suggest that the first approach is best to use for analysing the mechanism of microparticle and fluid manipulation in microfluidic devices.

Introduction

Integrating acoustics technologies such as surface acoustic wave (SAW) devices into microfluidic setups (often called

* Corresponding author.
E-mail address: mohammad.rahmati@northumbria.ac.uk (M. Rahmati).

https://doi.org/10.1016/j.ijengsci.2021.103563
Received 30 October 2020; Received in revised form 30 March 2021; Accepted 12 August 2021
Available online 1 September 2021
0020-7225/© 2021 The Authors. Published by Elsevier Ltd. This is an open access article under the CC BY license (http://creativecommons.org/licenses/by/4.0/).

acoustofluidics) to manipulate and control fluid and microparticles/droplets/cells has become one of the most popular areas of microfluidics research in recent years (Whitesides, 2006, J. Friend & L. Y. Yeo,2011 Huang, 2019, Li & Huang, 2018, Sackmann, Fulton & Beebe, Mar 13 2014, Beebe, Mensing & Walker, 2002, Franke, Abate, Weitz & Wixforth, 2009). These acoustofluidic systems offer great potentials to design and fabricate devices to address important challenges in the fields of biomedical engineering, biology, medicine and chemistry (Sackmann, Fulton & Beebe, Mar 13 2014, Beebe, Mensing & Walker, 2002, Ding et al., 2013, Schmid, Weitz & Franke, 2014, Chen, Toh, Chai & Yang, 2004). The advantages of using SAW devices as a part of microfluidic systems are their simple planar design, small size, efficiency and low cost. These devices offer reliable, precise and controllable manipulation with high biocompatibility in non-invasive and contact-free manner (Whitesides, 2006, Ding et al., 2013, Wang et al., 2017).

SAWs cause "acoustic streaming" (Ding et al., 2013, Sadhal, 2012), a phenomenon which happens when a traveling surface acoustic wave (TSAW) propagates through a liquid and the acoustic energy of the wave is transferred into the fluid. This results in a momentum transfer between the wave and the fluid which induces movement in the fluid and excites internal streaming. (Ding et al., 2013) Acoustic streaming can be used to deflect (Franke, Abate, Weitz & Wixforth, 2009), separate and sort (Schmid, Weitz & Franke, 2014, Franke et al., Mar 21 2010, Skowronek, Rambach & Franke, 2015), focus (Collins, Ma, Han & Ai, 2017), separate and capture (Collins et al., 2017, Sivanantha et al., 2014), trap (Rambach, Linder, Heymann & Franke, 2017), microparticles/cells, mix (Destgeer et al., 2014) and pump fluids and suspensions in microfluidic devices (Ding et al., 2013, Fu et al., 2017). A summary of using SAW acoustic streaming for microparticle, cell and fluid manipulation is shown in Table 1.

Numerical simulation of SAW based acoustofluidic systems can aid in understanding the underling physics of these complex multi-physics systems which is essential for designing and fabricating such devices (Chen, Toh, Chai & Yang, 2004, Walls & Abedian, 2014). There are previous studies on numerical simulation of acoustofluidic systems. For examples, Schmid, Weitz & Franke (2014) simulated particle deflection using acoustic streaming effect, and Collins, Ma, Han & Ai (2017) presented acoustic streaming flow field and fluid streamlines in two dimensions, both without modelling the acoustic field. However, few attempts have been made to assess the basis, strengths and limitations of various computational methods. Such an approach can help to optimise acoustofluidic devices and can potentially lead to development of novel devices.

Our study aims to investigate the effects of SAW induced acoustic streaming on fluid and microparticles using two different numerical simulation approaches. We compare and validate the results of both approaches with acoustofluidics experiments. The first approach is performed by modelling the whole acoustic field caused by the SAW propagating on the lower wall. In this case the acoustic streaming force will be calculated directly using the density and velocity resulted from the acoustic field. In the second approach which is an approximation method, the effects of acoustic streaming is studied without modelling the acoustic field. Instead, in this approach, a simplified version of the acoustic streaming force will be implemented in the governing equations of fluid flow as an external body force. Although this approximation method has its limitations, it has been used in as the more popular modelling approach to study the streaming effects in many of the previous studies (Schmid, Weitz & Franke, 2014, Collins, Ma, Han & Ai, 2017). In this paper, fluid flow and microparticles' movement are studied under different inlet and sheath flow rates and different acoustic power conditions.

A schematic of the acoustic streaming effect on a pure fluid and a microparticle suspension in a continuous microchannel flow is shown in Fig. 1. The acoustic field generates counter-rotation vortical structures which cause the flow to divert from its original straight path shown in Fig. 1(a). This streaming effect can help in mixing different flowing fluids inside a microchannel. To manipulate microparticles, the flowing system is designed in a way that without acoustic streaming the microparticles flow into the lower outlet, while operating the acoustic device results in the microparticles deflecting into the upper outlet as shown in Fig. 1(b).

Theoretical analysis of an acoustofluidic system

An acoustofluidic platform is a multi-physics system on different time and length scales consisting of fluid flow, SAWs, micro-

Table 1
Use of acoustic streaming effect to manipulate microparticles.

Manipulation Task	Objects	Research Group	Investigation
Directing	Polyacrylamide microparticles, Droplets	Franke et al. (Franke, Abate, Weitz & Wixforth, 2009)	Experimental
Separating & Sorting	Droplets, Cells: B16F10 mouse melanoma	Schmid et al. (Schmid, Weitz & Franke, 2014)	Experimental Simulation
	Cells: HaCaTcells, murine fibroblasts, L929 cells and, MV3 melanoma cells	Franke et al. (Franke et al., Mar 21 2010)	Experimental
	Polystyrene microparticles	Skowronek et al. (Skowronek, Rambach & Franke, 2015)	Experimental
Focusing	Polystyrene microparticles	Collins et al. (Collins, Ma, Han & Ai, 2017)	Experimental Simulation
Separating & Capturing	Polystyrene microparticles	Collins et al. (Collins et al., 2017)	Experimental
	Cells: healthy, Glutaraldehyde treated and, malaria-infected red blood cells	Sivanantha et al. (Sivanantha et al., 2014)	Experimental
Trapping	Droplets	Rambach et al. (Rambach, Linder, Heymann & Franke, 2017)	Experimental
Mixing	Dyed and pure water	Destgeer et al. (Destgeer et al., 2014)	Experimental

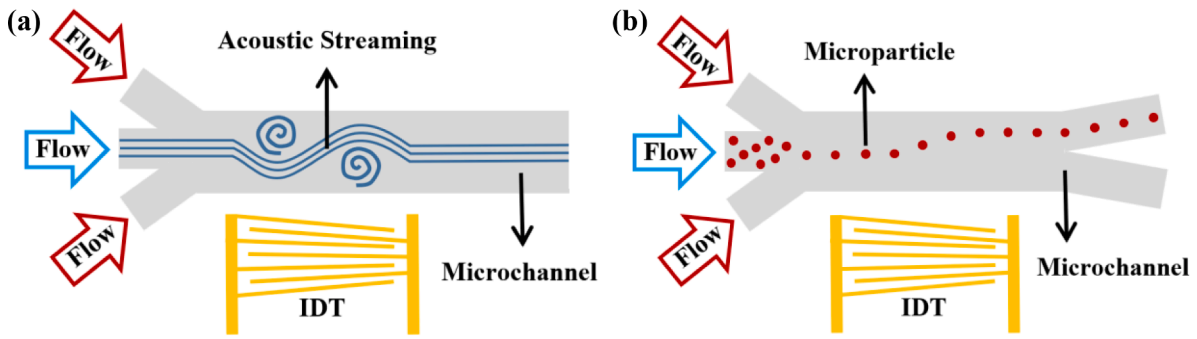

Fig. 1. A schematic of (a) acoustic streaming effect on a fluid in a co-flowing microfluidic channel and (b) deflection of a suspension of microparticles by acoustic streaming across the channel. Sheath flows from two side inlets focus the liquid form the main inlet in the middle of the channel.

particles suspended in the fluid and the interaction between the components. For a laminar flow, the governing equations of motion in three dimensions (i.e. the continuity and Navier-Stokes equations) are presented as follows:

$$\frac{\partial \boldsymbol{\rho}_f}{\partial \boldsymbol{t}} + \nabla . \boldsymbol{\rho}_f \boldsymbol{U}_f = 0 \tag{1}$$

$$\frac{\partial \boldsymbol{\rho}_f \boldsymbol{U}_f}{\partial \boldsymbol{t}} + (\boldsymbol{U}_f . \nabla)\boldsymbol{\rho}_f \boldsymbol{U}_f = -\nabla \boldsymbol{P} + \boldsymbol{\mu}_f \nabla^2 \boldsymbol{U}_f + \boldsymbol{G} + \boldsymbol{F}_{AS} \tag{2}$$

where ρ_f is the fluid density, $\boldsymbol{U}_f$ is the fluid velocity vector, t is the time, P is the fluid pressure, μ_f is the fluid viscosity, $\boldsymbol{G} = \rho_f \boldsymbol{g}$ is the gravity force and $\boldsymbol{F}_{AS}$ is the force fluid experiences due to the acoustic field Batchelor (2000).

Simplifying the continuity and Navier-Stokes equations for a steady incompressible fluid flow leads to:

$$\nabla . \boldsymbol{U}_f = 0 \tag{3}$$

$$\boldsymbol{\rho}_f \left((\boldsymbol{U}_f . \nabla) \boldsymbol{U}_f \right) = -\nabla \boldsymbol{P} + \boldsymbol{\mu}_f \nabla^2 \boldsymbol{U}_f + \boldsymbol{G} + \boldsymbol{F}_{AS} \tag{4}$$

SAWs are generated when an appropriate alternating electric field is exerted to a piezoelectric material. To do this a radio frequency (RF) signal is applied to the interdigital transducers (IDTs) which are patterned on the piezoelectric substrate. The signal's frequency should be equal to the wavelength (distance between the IDT's fingers) divided by the speed of sound in the piezoelectric substrate, to fulfil the resonance condition. As a result, the piezoelectric material contracts and expands periodically, transforming the electrical stress to mechanical stress. This continuous deformation of the piezoelectric substrate causes the production and propagation of the travelling surface acoustic wave along the surface of the substrate and perpendicular to the electrodes (Ding et al., 2013, Singh, Kumar & Chattopadhyay, 2015).

When a TSAW couples into a liquid, the difference between the wave propagation speed in the piezoelectric substrate and the liquid causes the wave's acoustic energy to refract into the fluid a phenomenon called acoustic refraction. By propagating into the fluid, the amplitude of this refracted wave starts to attenuate resulting in the generation of a "leaky wave". The refraction angle, which is called the Rayleigh angle, is calculated using the ratio of the speed of sound in the piezoelectric substrate to the speed of sound in the liquid (Ding et al., 2013).

$$\boldsymbol{\theta}_{\boldsymbol{R}} = \arcsin\left(\frac{\boldsymbol{c}_f}{\boldsymbol{c}_s}\right) \tag{5}$$

where $c_f$is the wave speed in the fluid and c_s is the wave speed in the piezoelectric substrate (Ding et al., 2013). The refracted longitudinal waves induce movement in the fluid by generating a force in the waves' propagation direction. The boundaries reflect the moving fluid and cause internal streaming. This phenomenon is called acoustic streaming (Ding et al., 2013, Sadhal, 2012).

Modelling acoustic streaming effects using acoustic field variables (first approach)

The analytical study on acoustic streaming effect was first introduced by Nyborg (1953) and was later improved by Lighthill (1978). The acoustic streaming forces are calculated in a fluid assuming a steady state for both the acoustic and flow fields using a perturbation method (Nyborg, 1953, Lighthill, 1978, Shiokawa, Matsui & Ueda, 1990).

$$\boldsymbol{P} = \boldsymbol{P}_0 + \boldsymbol{P}_a + \boldsymbol{P}_b \tag{6}$$

$$\rho_f = \rho_0 + \rho_a + \rho_b \ \textit{with}\ \rho_a = \frac{P_a}{{c_f}^2} \tag{7}$$

$$U_f = U_0 + U_a + U_b \tag{8}$$

where 0, a and b indices denote unperturbed state, first order and second order approximations of the three variables. Substituting the above equations in Eqs. (1) and (2) of the fluid flow and solving for the first and second order equations results in the acoustic field equations. The acoustic streaming force, F_{AS}, acts as a body force on the fluid and is calculated using the second order source terms of the equations as follows:

$$F_{AS} = \langle \rho_a \partial_t U_a \rangle + \rho_f \langle (U_a . \nabla) U_a \rangle \tag{9}$$

where $\langle \Psi \rangle$ denotes the time average of Ψ (Nyborg, 1953, Lighthill, 1978, Shiokawa, Matsui & Ueda, 1990). Using the first order continuity equation, the above can be further simplified to:

$$F_{AS} = \rho_f \langle U_a (\nabla . U_a) \rangle + \rho_f \langle (U_a . \nabla) U_a \rangle \tag{10}$$

The acoustic streaming force components from Eq. (10) are calculated as follows:

$$F_{ASx} = \left(\frac{\rho_f}{2} U_{ax} \left(\frac{\partial U_{ax}}{\partial x} + \frac{\partial U_{ay}}{\partial y} \right) \right) + \left(\frac{\rho_f}{2} \left(U_{ax} \frac{\partial U_{ax}}{\partial x} + U_{ay} \frac{\partial U_{ax}}{\partial y} \right) \right) \tag{11}$$

$$F_{ASy} = \left(\frac{\rho_f}{2} U_{ay} \left(\frac{\partial U_{ax}}{\partial x} + \frac{\partial U_{ay}}{\partial y} \right) \right) + \left(\frac{\rho_f}{2} \left(U_{ax} \frac{\partial U_{ay}}{\partial x} + U_{ay} \frac{\partial U_{ay}}{\partial y} \right) \right) \tag{12}$$

where U_{ax} and U_{ay} are the wave velocities in x- and y-directions, respectively. For the TSAW propagating in x-direction with velocity components of $U_{a_x} = \overline{U}_{a_x} e^{i\omega t}$ and $U_{a_y} = \overline{U}_{a_y} e^{i\omega t}$ (ω is the wave angular frequency), the acoustic streaming force components are derived from Eq. (9) as:

$$F_{AS_x} = \left(\frac{P_a}{2{c_f}^2} \omega \overline{U}_{a_x} \right) + \left(\frac{\rho_f}{2} \left(\overline{U}_{a_x} \frac{\partial \overline{U}_{a_x}}{\partial x} + \overline{U}_{a_y} \frac{\partial \overline{U}_{a_x}}{\partial y} \right) \right) \tag{13}$$

$$F_{AS_y} = \left(\frac{P_a}{2{c_f}^2} \omega \overline{U}_{a_y} \right) + \left(\frac{\rho_f}{2} \left(\overline{U}_{a_x} \frac{\partial \overline{U}_{a_y}}{\partial x} + \overline{U}_{a_y} \frac{\partial \overline{U}_{a_y}}{\partial y} \right) \right) \tag{14}$$

Modelling acoustic streaming effects by approximation (second approach)

Eqs. (9) to (14) model the acoustic streaming force using the first order density and velocity caused by the acoustic filed. In order to simplify the acoustic streaming force as the microchannel's height is consideably smaller than its width, the wave's velocity component is the y-direction is negligible, so, we consider a one-dimensional attenuating travelling SAW propagating in x-direction. The wave velocity can be written as:

$$U_{ax} = U_{ac} e^{-(\alpha + ik)x} e^{i\omega t} \tag{15}$$

where U_{ac} is the wave velocity amplitude, α is the attenuation parameter, $k = \frac{2\pi}{\lambda}$ is the wavenumber and x is the fluid location along the wave propagation direction. Substituting Eq. (15) in Eq. (10), we can derive the acoustic streaming force without the need for the first order density and velocity caused by the acoustic field as:

$$F_{AS} = -\alpha \rho_f {U_{ac}}^2 e^{-2\alpha x} \tag{16}$$

Using the wave intensity $I_{ac} = \frac{1}{2}\omega^2 A^2 \rho_f c_f$ in Eq. (16):

$$F_{AS} = -\sigma {c_f}^{-1} I_{ac} e^{-\sigma x} \tag{17}$$

where $\sigma^{-1} = \frac{1}{2\alpha}$ is the fluid attenuation length, and A is the wave displacement amplitude (Schmid, Weitz & Franke, 2014, Nyborg, 1953, Lighthill, 1978, Shiokawa, Matsui & Ueda, 1990). As mentioned before, the TSAWs are refracted into the liquid along the Rayleigh angle so the acoustic streaming force is in the Rayleigh wave direction:

$$F_{ASx} = -\alpha \rho_f {U_{ac}}^2 e^{-2\alpha x} \sin\theta_R \tag{18}$$

$$F_{ASy} = -\alpha \rho_f {U_{ac}}^2 e^{-2\alpha x} \cos\theta_R \tag{19}$$

The acoustic streaming force acts as a body force on the fluid Ding et al., 2013) and thus Eqs. (11) to ((14) or (18) and (19) are substituted as the term F_{AS} in Eq. (4).

Modelling the microparticles and acoustic radiation force

To study the dispersed microparticle phases, two main approaches are used: the Euler-Lagrange approach and the Euler-Euler approach (Crowe, Schwarzkopf, Sommerfeld & Tsuji, 2011, Crowe, 2005). In this research, to study a multiphase flow of one primary phase of continuous fluid and secondary phases of dispersed microparticles are of interest, the Euler-Lagrange approach is used. This approach, provides detailed information of position and velocity for each particle (Crowe, Schwarzkopf, Sommerfeld & Tsuji, 2011, Crowe, 2005). Using the Euler-Lagrange approach, the governing equations of motion for a single particle are as follows:

$$\frac{\partial \boldsymbol{X_p}}{\partial \boldsymbol{t}} = \boldsymbol{U_p} \tag{20}$$

$$\frac{\partial \boldsymbol{\rho_p U_p}}{\partial \boldsymbol{t}} = \boldsymbol{\rho_p}\frac{\boldsymbol{U_f} - \boldsymbol{U_p}}{\boldsymbol{\tau_p}} + \boldsymbol{W} + \boldsymbol{F_{AR}} \tag{21}$$

where $\boldsymbol{X_p}$ is the particle's position, ρ_p is the particle density, $\boldsymbol{U_p}$ is the particle velocity vector, $\boldsymbol{W}$ is the gravity force on the particle and $\boldsymbol{F_{AR}}$ is the acoustic force acting on the particle. The first term on the right-hand side of Eq. (19) is the drag force that the particles experience when moving through the fluid which depends on the properties of the fluid, the properties of the particles and the velocity of the particle relative to the flow. $\tau_p (= \rho_p d^2/18\mu_f)$ is the particle characteristic time which is the time for the particle to respond to a velocity change (Crowe, Schwarzkopf, Sommerfeld & Tsuji, 2011, Crowe, 2005).

In the presence of an acoustic field, the acoustic energy refracted into the fluid affects the particles suspended in the fluid medium as well. This interaction is called the acoustic radiation force (Ding et al., 2013). For the TSAW, this force directs each particle along the wave's propagation direction King (1934). The analytical study on acoustic radiation force was first introduced by King (1934) when he calculated the acoustic radiation force on rigid spheres ignoring the fluid viscosity and using perturbation methods. Yosioka & Kawasima (1955) successfully extended the calculations for compressible spheres accounting for the effects of microparticles compressibility. These studies were then summarised and generalised by Gorkov (1962). Doinikov (1994, Doinikov, 1994) further improved calculation of the acoustic radiation force on a rigid (Doinikov, 1994) and compressible (Doinikov, 1994) sphere by accounting for the viscous effects of the fluid.

The acoustic radiation force, $\boldsymbol{F_{AR}}$, acting on a spherical particle suspended in a fluid in a TSAW field is described as follows:

$$\boldsymbol{F_{AR}} = f_2^i(\widetilde{\rho}, \widetilde{\delta})\pi r^3 \rho_f \langle \boldsymbol{V_{in}}.\nabla \boldsymbol{V_{in}}\rangle \boldsymbol{k} \text{ with } \widetilde{\rho} = \frac{\rho_p}{\rho_f} \text{ and } \widetilde{\delta} = \frac{\delta}{r} \tag{22}$$

$$f_2^i(\widetilde{\rho}, \widetilde{\delta}) = \frac{6(1-\widetilde{\rho})^2(1+\widetilde{\delta})\widetilde{\delta}}{(1+2\widetilde{\rho})^2 + 9(1+2\widetilde{\rho})\widetilde{\delta} + \frac{81}{2}\left(\widetilde{\delta}^2 + \widetilde{\delta}^3 + \frac{1}{2}\widetilde{\delta}^4\right)} \tag{23}$$

where $\boldsymbol{r}$ is the particle radius, $\boldsymbol{V_{in}}$ is velocity field of the incoming wave, $\boldsymbol{k}$ is the wave vector, and δ is the thickness of the viscous, acoustic boundary layer (King, 1934, Yosioka & Kawasima, 1955, Gorkov, 1962, Doinikov, 1994, Doinikov, 1994, Settnes & Bruus, 2012). The terms with higher powers of $\widetilde{\delta}$ are ignored for calculation simplicity (King, 1934, Yosioka & Kawasima, 1955, Gorkov, 1962, Doinikov, 1994, Doinikov, 1994, Settnes & Bruus, 2012).

For a one directional TSAW propagating in x-direction, the force is presented as follows:

$$F_{ARx} = f_2^i(\widetilde{\rho}, \widetilde{\delta})\pi r^3 E_{ac} k \tag{24}$$

where $E_{ac} = \frac{1}{2}\beta_f {P_{ac}}^2$ is the acoustic energy density of the wave, β_f is the fluid compressibility and P_{ac} is the acoustic pressure amplitude (King, 1934, Yosioka & Kawasima, 1955, Gorkov, 1962, Doinikov, 1994, Doinikov, 1994, Settnes & Bruus, 2012).

If the effects of fluid viscosity are negligible, the acoustic radiation force is reduced by a factor of $(kr)^3$. If the effects of compressibility of the particles are negligible as well, the acoustic radiation force for a travelling acoustic wave is calculated using the following equations:

$$F_{ARx} = \left(\frac{2\pi^3 {P_{ac}}^2 {\forall_p}^2 \beta_f}{\lambda^4}\right)\varnothing_t(\rho) \tag{25}$$

$$\varnothing_t(\rho) = \frac{9 + 2\left(1 - \rho_f/\rho_p\right)^2}{\left(2 + \rho_f/\rho_p\right)^2} \tag{26}$$

where $\forall_p$ is the particle volume (King, 1934, Yosioka & Kawasima, 1955, Gorkov, 1962, Doinikov, 1994, Doinikov, 1994, Settnes & Bruus, 2012, Liu et al., 2017, Nilsson, Petersson, Jonsson & Laurell, Apr 2004, Doinikov, 2003).

Computational setup

The numerical modelling of the problem was done using a commercial software package COMSOL Multiphysics (Version 5.3) which has an integrated finite-element solver. To simulate the three components of the problem, the SAW field, the fluid flow and the particle phase, the three modules of "pressure acoustics", "laminar flow" and "particle tracing" are used. For modelling the computational domain, the geometry is defined as a three-dimensional rectangular microchannel (length: 1000 μm (z-direction), width: 200 μm (x-direction), height: 50 μm (y-direction)) and is discretized with a structured hexahedron grid with nearly 40000 elements. The discretized computational domain is shown in Fig. 2.

Since the volume fraction of the dispersed microparticle phase is smaller than the volume fraction of the continuous fluid phase, it is assumed that the fluid particle mixture is sparsely distributed. As the sizes of the microparticles are insignificant compared to the microchannel dimensions and the velocities of the microparticles are low, it is assumed that a "one-way coupling" occurs between the two phases (fluid and particle), which means that the continuous phase affects the dispersed phase but not vice-versa (COMSOL 2018).

When simulating the physics of the fluid flow, the flow is considered steady in time, laminar, incompressible and viscous. The Navier-Sokes equations (i.e. Eqs. (3) and (4)) are used to model the flows. The finite element method (FEM) is used for the discretization of the governing equations.. The generalized minimal residual (GMRES) iterative is used to solve the governing equations of the multiphysics system.

Two different approaches are used to apply the effect of surface acoustic waves to the problem. For the first approach, the acoustic streaming effects are directly calculated by modelling the acoustic field using the SAW propagating on the lower wall. In this case the acoustic streaming force is calculated using the first order density and velocity resulted from the acoustic field, i.e., Eqs. (13) and (14), then implemented in the governing equations. While in the second approach, the effect of the induced acoustic streaming acting on the fluid is accounted by substituting the velocity of a one-dimensional attenuating TSAW in the acoustic streaming force formula, i.e. Eqs. (18) and (19), as an external body force in the flow's governing equations. This approach is an approximation method for the effects caused by SAW streaming when the height of the microchannel is consideably smaller than its width.

In the case of the particles existing in the flow filed, the acoustic radiation force caused by the TSAW is added to the simulation as an external body force on the particles. Due to the fluid flow, a viscous drag force is applied to the particles, modelled by the Stokes drag force. The differential equations that govern the particle motion are solved for each particle in three dimensions. At each time step, the acoustic radiation and drag forces affecting the particle movement are calculated based on the acoustic and fluid fields, respectively. Finally, the particles' positions are continuously tracked and this process is repeated until it reached the specified end time of the simulation (COMSOL 2018).

Acoustic modelling boundary conditions

The TSAW propagation was modelled using a boundary condition for the lower wall. The velocity of the SAW propagating on the active portion of the lower wall is defined as follows:

$$\boldsymbol{u}_{x-wall} = \boldsymbol{A}_y \boldsymbol{\xi} \boldsymbol{\omega} \boldsymbol{e}^{-\boldsymbol{\alpha}(0.5w-x)} \boldsymbol{e}^{\boldsymbol{i}[-\boldsymbol{k}(0.5w-x)]} \tag{27}$$

$$\boldsymbol{u}_{y-wall} = \boldsymbol{A}_y \boldsymbol{\omega} \boldsymbol{e}^{-\boldsymbol{\alpha}(0.5w-x)} \boldsymbol{e}^{\boldsymbol{i}[-\boldsymbol{k}(0.5w-x)-0.5\pi]} \tag{28}$$

where u_{x-wall} and u_{y-wall} are the SAW velocity in x- and y-directions, respectively, A_y is the wave's displacement amplitude in y-direction, w is the channel width, x is the longitudinal direction and $\zeta = A_x/A_y$ is the ratio of the displacement amplitudes in x- and y-directions (Devendran et al., 2016). All the other walls were modelled using an impedance boundary condition as follows:

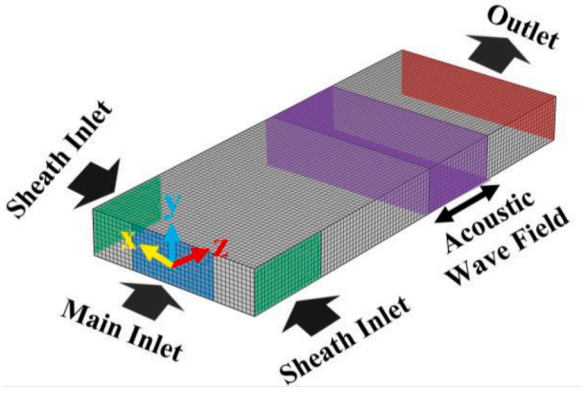

Fig. 2. A view of the computational domain and mesh. Main inlet (coloured blue) at the middle of the front side, sheath inlets (coloured green) on the two sides, outlet (coloured red) at the back and the flow is in z-direction. The acoustic wave field is coloured purple and the acoustic wave travels in x-direction, the height of the microchannel is in y-direction.

$$Z_{wall} = \rho_{wall} c_{wall} \tag{29}$$

where Z_{wall} is the wall's impedance, ρ_{wall} is the wall density and c_{wall} is the wave's propagation velocity in the wall.

Flow modelling boundary conditions

The following boundary conditions are defined to model the physics of the flow field:

- On solid walls $\boldsymbol{U} = \boldsymbol{U}_{wall}$ (no-slip boundary condition).
- At the flow inlet/sheath mass or volume flow rate is known.
- At the flow outlets mass or volume flow rate is known.

Experimental setup

In order to verify the simulation results, experiments are designed and performed. To do that, a polydimethylsiloxane (PDMS) microchannel (length: 1000 μm (z-direction), width: 200 μm (x-direction), height: 50 μm (y-direction)) with three inlets and one outlet is placed on a SAW device made of lithium niobate ($LiNbO_3$) piezoelectric substrate and one single slanted IDT with a frequency range of 161 MHz to 171 MHz, which generated a TSAW. Slanted IDTs (also known as tapered IDTs) have a very broad bandwidth with a range of varying frequencies. These IDTs are operated by changing the electrode periodicity and are capable to deflect a moving particle or droplet by continuously changing the operating frequency (Schmid, Weitz & Franke, 2014, Fu et al., 2017). For the following experiments, a slanted IDT with a frequency of 164 MHz is used to position the acoustic sound path, however a straight IDT with the same position and frequency can be used as well.

The SAW setup is placed on a holder and then positioned over an inverted microscope (Olympus IX73). Videos are recorded using a high speed camera (Photron, UX50). The micrograph of the SAW setup is presented in Fig. 3. It shows a part of the IDT on the bottom, the main and sheath inlets of the microchannel on the right and the outlet on the left (flow direction is from left to right). An RF signal generator (Rohde & Schwarz, SMB100A) is connected to the SAW device and set the input power and frequency. Three syringe pumps (Harvard Apparatus, PHD2000) are connected to the inlets to control the flow rates of the inlet and sheath flows and the outlets are connected to individual vials to collect the exiting fluid. The experiment is controlled with a desktop computer which is also used for analysis of the captured videos.

To study the acoustic streaming, two different cases of experiments are performed. In the first case to visualise acoustic streaming in a microchannel flow, de-ionized (DI) water dyed with trypan blue colour is injected in the microchannel through the main inlet and pure water is injected in the flow field as sheath flows through side inlets. The properties of both the pure water and the dyed water are defined as density ρ_f=998 kg/m^3, viscosity μ_f=0.001 kg/(m.s) and compressibility β_f=4e^{-10} Pa^{-1}.

In the second case to investigate the effects of acoustic streaming on microparticles, spherical polystyrene microparticles (with diameter d=1 μm and density ρ_p=1050 kg/m^3) dispersed in water as the carrier fluid are injected in the microchannel through the main inlet and pure water is injected in the flow field as sheath flows through side inlets. To collect the experimental data, 400 images are taken and superimposed to visualize the particle trajectories for each case. The effects of different inlet and sheath flow rates as well as different acoustic powers are studied. The particle velocity values are extracted from the videos with a digital particle image velocimetry (PIV) method using a MATLAB toolbox named PIVlab (Thielicke & Stamhuis, 2014, Thielicke, 2014, Thielicke & Stamhuis, 2018).

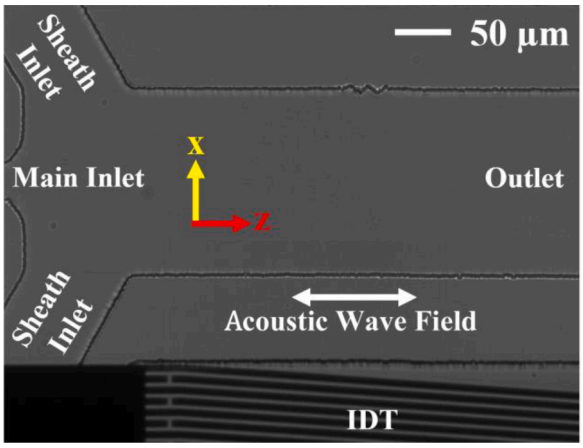

Fig. 3. A micrograph of the SAW setup. A part of the IDT on the bottom, the main and sheath inlets of the microchannel on the left and the outlet on the right (the flow direction is from left to right) is visible. The acoustic sound path is indicated by a double arrow.

Results and discussions

Investigation of the acoustic and fluid flow field parameters

In order to verify the numerical simulation, velocity components in z- and x-directions and the velocity magnitude and vorticity magnitude in xz-plane from the simulations are compared with the data extracted from the experimental videos at the centre of the microchannel. The comparison graphs are presented in Fig. 4 for the acoustic power of 65 mW and the main inlet volume flow rate and each sheath flow volume flow rates are 25.0 μl/hr and 50.0 μl/hr, respectively.

The graphs obtained from the experimental and both simulation approaches show agreements among each other. The results for the velocity component in z-direction (Fig.4(a)) from the first simulation approach follows the experimental data trend more accurately compared to the second simulation approach. According to Fig. 4(a), the value for the z-velocity first increases and then decreases in the acoustic field for both the experiment and first approach. However, for the second approach, the trend for the z-velocity is reversed in the acoustic field. The difference in the maximum and minimum values of the graph for the second approach is smaller compared to the other two graphs since the second approach underestimates the maximum/minimum value by 14 percent. This difference is expected as the second approach approximates the first approach. The results for the velocity component in the x-direction (Fig. 4(b)) is consistent with the experimental data for both simulation approaches. However, the second approach overestimates the maximum value by 19 percent. For the first simulation approach, the velocity magnitude in xz-plane (Fig. 4(c)) shows a more accurate agreement between the experimental data and the simulation data, compared to those from the second approach. For both the experiment and first approach the velocity magnitude in the acoustic field, first increases and then decreases. The velocity magnitude in the acoustic field increases to a near constant value for the second approach. For the vorticity magnitudes in xz-plane (Fig. 4(d)), these graphs show good agreements with each other. It can be seen from Fig. 4(d) that both the computational approches predict the vorticities at the beginning and the end of the acoustic field accurately. However, through the width of the acoustic field (i.e., the zoomed section in Fig. 4(d)) the first approach predicts the vorticity changes in the acoustic field similar to the experimental data, whereas for the second approach, the vorticity is nearly zero through the width of the acoustic field.

Fig. 5 comapres the velocity components in y-direction, total velocity magnitude, pressure and shear rate graphs along the centreline of the microchannel given by the two different acoustic simulation approaches. The acoustic power is 65 mW, and the main inlet volume flow rate and each sheath flow volume flow rates are 25.0 μl/hr and 12.5 μl/hr, respectively. By comparing the graphs for the two computational methods, we see how the flow field parameters are changed along the centreline of the microchannel. The velocity

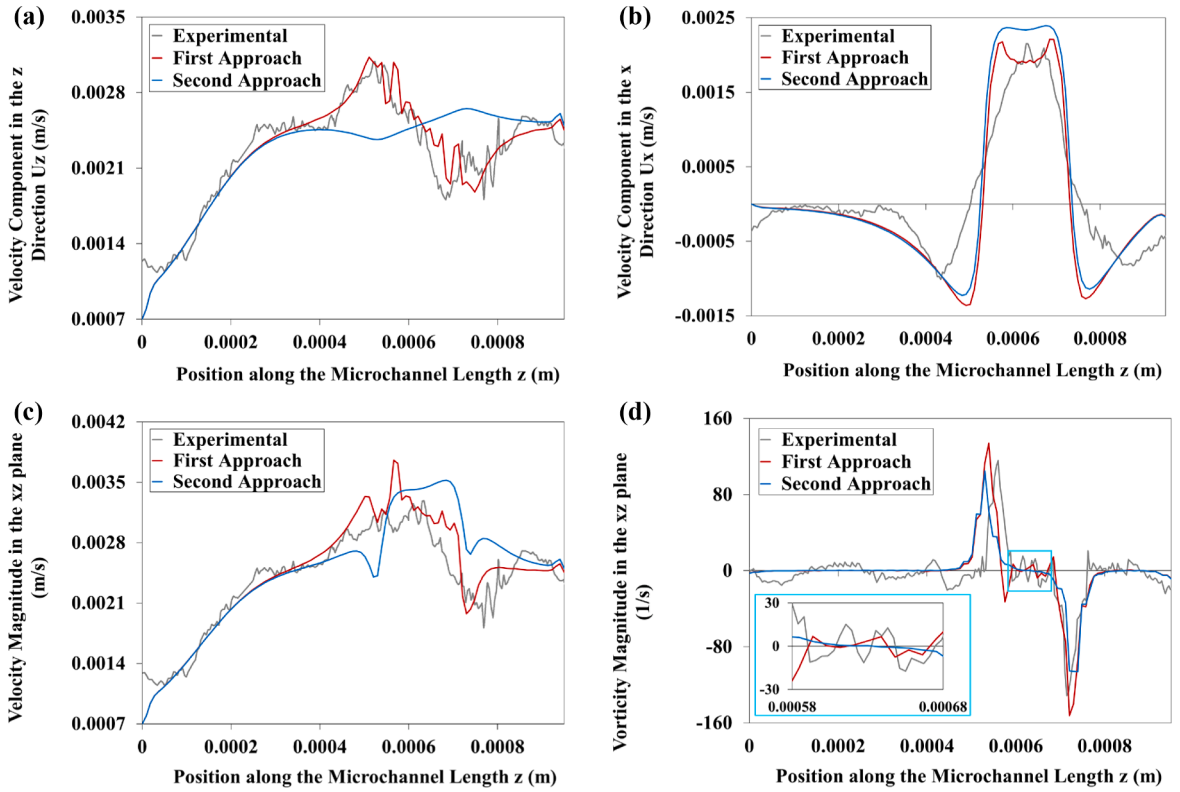

Fig. 4. Velocity component in (a) z-direction and (b) x-direction, (c) velocity magnitude and (d) vorticity magnitude in x-z plane along the z-direction (length) of the microchannel for the acoustic power of 65 mW, the main inlet volume flow rate of 25 μL/hr and each of the sheath flow volume flow rates of 50 μL/hr from the experimental, first and second computational approach.

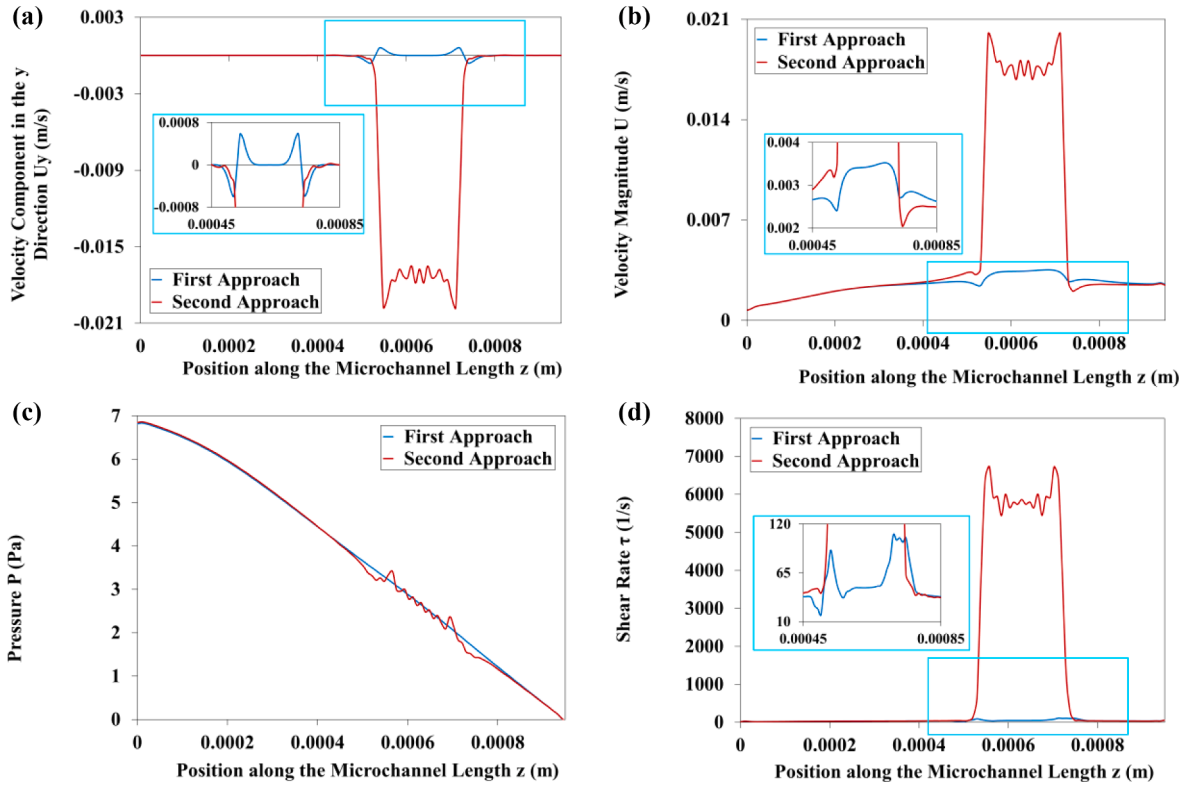

Fig. 5. (a) Velocity component in y-direction, (b) Velocity magnitude, (c) Pressure and (d) Shear rate along the centreline of the microchannel for the acoustic power of 65 mW, the main inlet volume flow rate of 25 μL/hr and each of the sheath flow volume flow rates of 50 μL/hr and for first and second computational approaches.

component in y-direction (Fig. 5(a)) is drastically different between the first and second approaches. The peak of y-velocity graph is 25 times larger for the first approach compared to the second approach. This is due to the differences in calculating acoustic streaming effects in y-direction for each simulation approach. The total velocity magnitude (Fig. 5(b)) is smooth and follows the trend for the typical pipe flow velocity graph for the second approach, with a small peak in the SAW field area caused by the body force acted on the fluid there. However, for the first approach, the graph for velocity follows the same trend but has a very sharp and jagged peak with a value 6 times larger compared to the second approach because the difference between y-component of the velocity for first and second approaches. The pressure (Fig. 5(c)) is smooth and looks like the typical pipe flow pressure graph for the second approach, whereas for the first approach it follows the same trend but then becomes uneven in the SAW field area because of the oscillatory velocity of SAW on the lower wall. The shear rates (Fig. 5(d)) for both the computational methods follow the same trend as well. However, for the first approach the peaks are 50 times larger compared to the second approach because of the SAW fields being completely modelled.

The simulation results for the pressure field contours at the bottom layer $y = -25$ μm, middle layer $y = 0$ μm and top layer $y = 25$ μm of the microchannel as well as velocity contours and vectors at middle layer $y = 0$ μm of the microchannel given by the two different acoustic simulation approaches is shown in Fig. 6. Here the acoustic power is 65 mW, and for the two different flow conditions, the main inlet volume flow rate is 25.0 μl/hr and each of the sheath flow volume flow rates is 50.0 μl/hr.

The pressure fields are changed from bottom to top in the presence of the SAWs as shown in Figs. 6(a-1) and 6(b-1). The pressure field results for both the computational approaches are similar outside the SAW field. However, inside the SAW field the difference in the pressure fields are quite noticeable. For the first computational approach, there seems to be a lot of fluctuations in the pressure field in the SAW region, due to the sinusoidal SAW patterns on the bottom wall of the channel. However, for the second computational approach, the pressure field in the SAW region changes smoothly through the width of the channel as the acoustic streaming force changes in that direction.

The first approach estimates the pressure field resulting from the SAW, more accurate flow field parameters and the change in the flow field parameters through the height of the channel. While the second approach is more efficient in terms of computational cost and time while still presenting good results. The need for a more accurate prediction (i.e. the results from the first approach) would be significant in different situations. First, when the microparticles are smaller and/or lighter and thus can be pushed to the top of the microchannel more easily due to the vertical component of the streaming force. Second, when the height of the microchannel and/or the width of the acoustic field are larger and thus the micropartilces are under the effect of the vertical component of the streaming force for a longer time. In these situations understanding what happens in the vertical direction is essential. The computational results for velocity contours and vectors from both the first and the second approaches is shown in Figs. 6(a-2) and 6(b-2). The results seem to

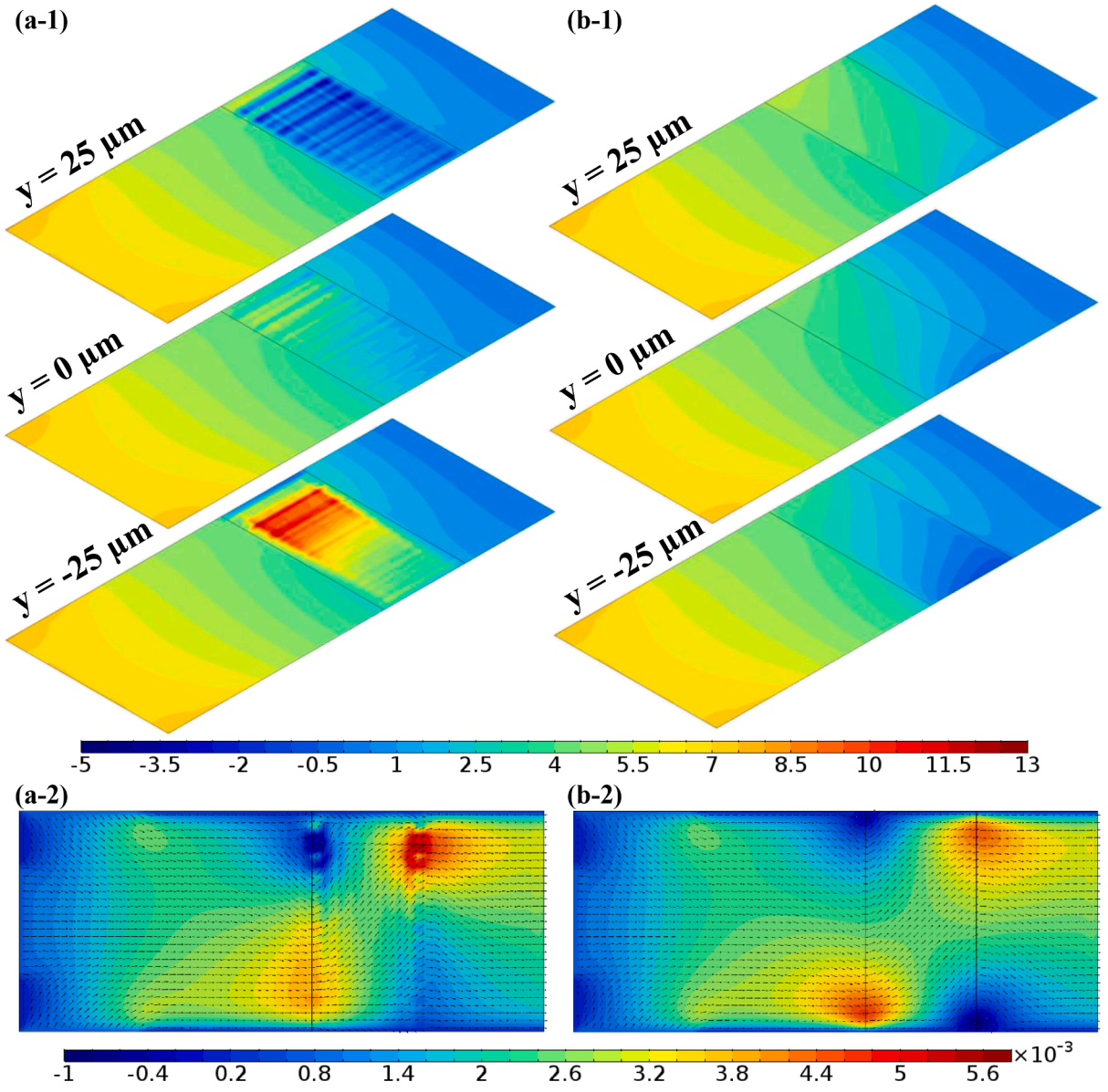

Fig. 6. Simulation results using (a) the first approach and (b) the second approach for (1) the pressure (Pa) field contours at the bottom y=-25 μm, middle y=0 μm and top y=25 μm of the microchannel and (2) velocity (m/s) contours and vectors at microchannel middle y=0 μm for main inlet volume flow rate and each of the sheath flow volume flow rates of 25.0 μL/hr and 50.0 μL/hr and with acoustic power of 65 mW.

be in good agreement with each other for every case. While for the second approach, the contours are smoother than the first approach.

Comparing the First and Second Computational Approaches

Figs. 7(a) and (b) present the comparisons among the velocity components in x-direction inside the microchannel with two different heights of 25 μm and 37 μm, resulted from the first and second computational approaches. Here the acoustic power is 65 mW, the main inlet volume flow rate and each sheath flow volume flow rates are 25.0 μl/hr and 50.0 μl/hr, respectively. For microchannels with heights of 50 μm (Fig. 4(b)), 37 μm (Fig. 7(a)), and 25 μm (Fig. 7(b)), the percentage of the difference between the values for the x-velocity are 19%, 17% and 16%, respectively. It is evident that as the height of microchannel decreases, the difference between the values for the velocity components in the x-direction decreases as well. We can conclude that for small heights of the microchannel (here 50 μm and below), both the computational approaches result in similar values for the velocity components in the x-direction.

Choosing one of the computational approaches over the other depends on a number of factors. If the purpose of the study is to investigate the acoustic field in details (especially through the width and height of the acoustic field), then the first computational

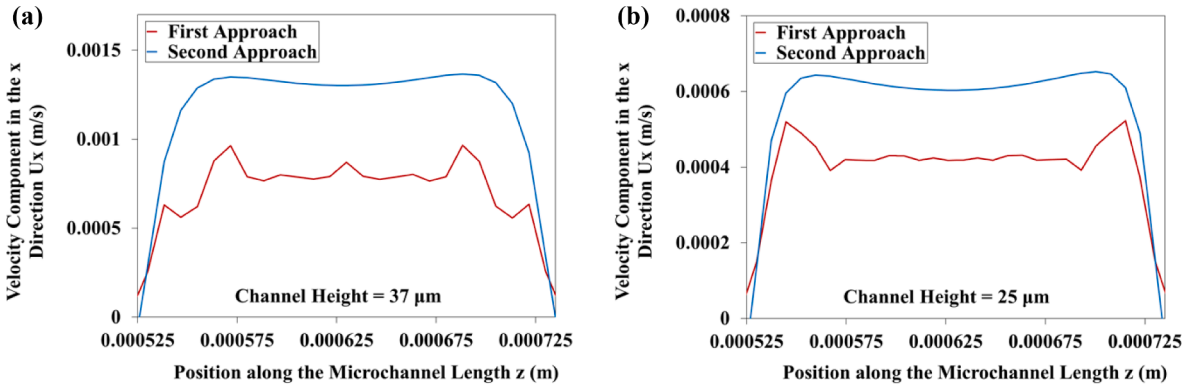

Fig. 7. Velocity component in the x-direction along the z-direction (length) of the acoustic field with a height of (a) 37.0 μm and (b) 25.0 μm for the acoustic power of 65 mW, the main inlet volume flow rate of 25 μL/hr and each of the sheath flow volume flow rates of 50 μL/hr from the first and second computational approaches.

approach is the best choice. If the height of the microchannel is small enough (here 50 μm and below), the second computational approach can be used to estimate the in-plane (i.e., xz-plane) parameters. However, to study the out-of-plane (i.e., y-direction) parameters, it is essential to use the first computational approach.

The Reynolds number of the flow, $Re = \frac{\rho_f U_f L}{\mu_f}$, where L is the length scale, combines the effects of the channel dimensions, flow velocity and fluid properties. For water flowing in the microchannel with the height of 50 μm with the main inlet and sheath flow volume flow rates of 25.0 μl/hr and 50.0 μl/hr, the Reynolds number is equal to 0.2. Such a low Reynolds number shows that the fluid flow is in the creeping flow regime where the viscous forces are dominant. In this study for cases with $Re \leq 0.2$, the second computational approach can be used for modelling the system.

In addition, if the acoustic field is present through the duration of the experiment and thus affects the domain for a large time frame, the first computational approach is the better option .Whereas the second computational approach can be used if the acoustic field is turned on as a pulse signal within a short time frame.

Acoustic steaming in a microchannel flow

The experimental data and the computational results obtained using the two different approaches are shown in Fig. 8. The results presented are for two different acoustic powers of 16.3 mW and 65 mW and with two different flow conditions, i.e., the main inlet volume flow rates of 25.0 μl/hr and 12.5 μl/hr and sheath flow volume flow rates of 50.0 μl/hr and 25.0 μl/hr, respectively.

The experimental and computational fluid flow fields presented in Fig. 8 are in good agreements with each other for every case. It can be seen in each case that for fixed volume flow rates of main and sheath inlets, increasing the acoustic power results in the increase in the acoustic streaming effect in both the experimental and computational flow fields. Also, for any fixed acoustic power, decreasing the volume flow rates results in the increase in the acoustic streaming effect in both the experimental and computational flow fields. The formation of two vortices at the channel sides under the effect of surface acoustic wave field is clearly observed through the simulation which is shown in Figs. 8(b-2-ii) and 8(c-2-ii). The flow changes its direction even before encountering the acoustic field as displayed in Fig. 4. The reason for this behaviour is mainly because of the low speed of the flow and continuity of fluid in this acoustofluidic problem.

For the first computational approach, the whole acoustic field resulted from the SAW is simulated and coupled to the flow field to obtain the results. This results in a more uneven streamline pattern in the SAW due to the change of flow field parameters caused by the SAW field. Whereas for the second computational approach, the acoustic field is not simulated and the effect of SAW on the flow field is modelled using only a body force. This causes the streamlines to be smoothened in the SAW area.

The effects of acoustic steaming on microparticles

The experimental and the computational results for microparticle tracks with the two different approaches are shown in Fig. 9. The results presented are for two different acoustic powers of 16.3 mW and 65 mW and with two different flow conditions with main inlet volume flow rate of 25.0 μl/hr and each of the sheath flow volume flow rates of 50.0 μl/hr. The experimental and computational particle trajectories seem to be in agreements with each other. It is seen in Fig. 8 that increasing the acoustic power results in the increase in the streaming effect in both the experimental and computational results.

For the two computational approaches, while the acoustic streaming force is modelled differently, the acoustic radiation force is the same. Therefore, any difference in the particle trajectories are caused by the difference in the modelling of the acoustic streaming force. By studying the experimental and computational flow fields and microparticle trajectories, we conclude that the microparticles small in size follow the streamlines of the flow field.

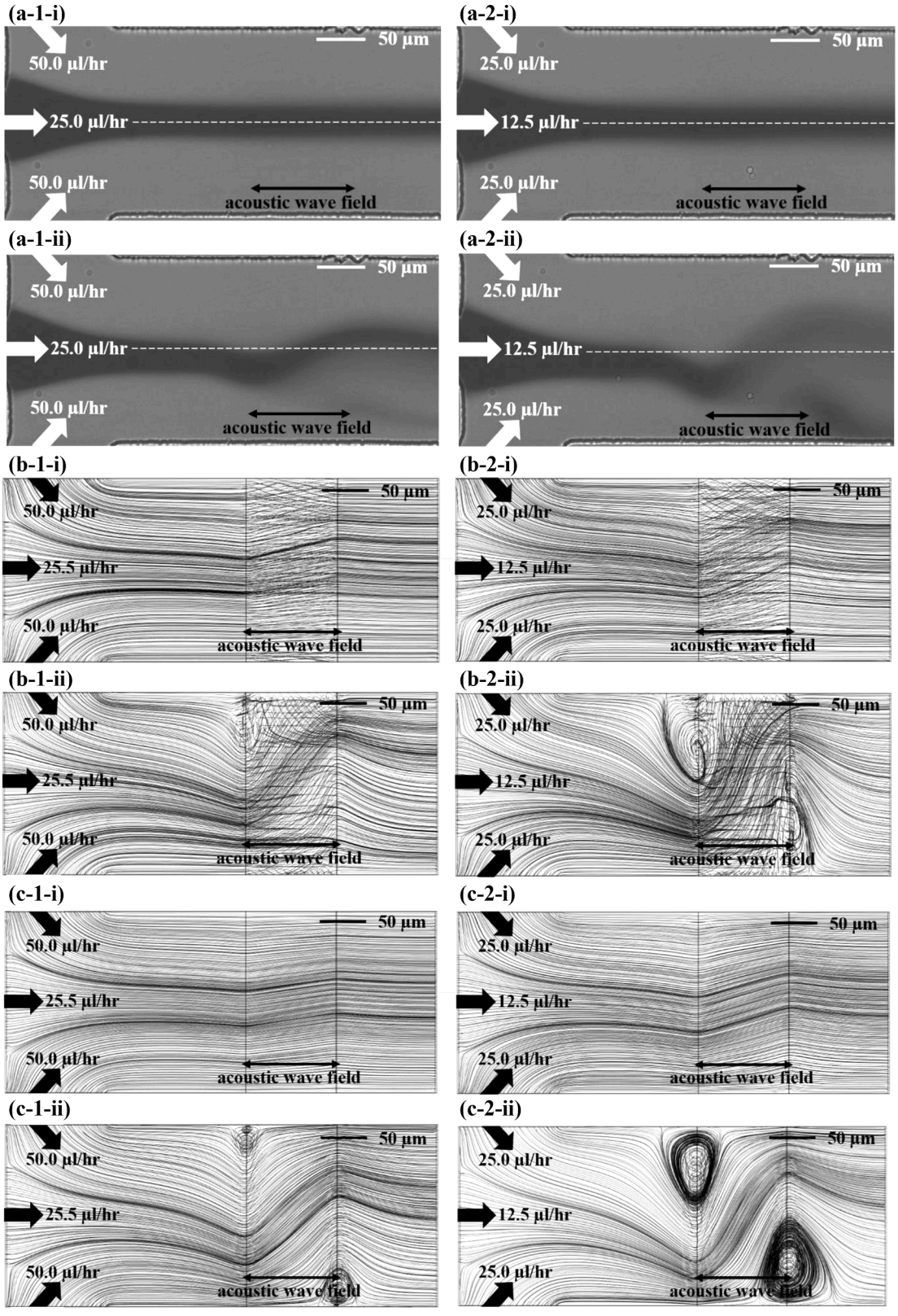

(caption on next page)

Fig. 8. Flow field results of (a) experimental, (b) computational with the first approach and (c) computational with the second approach for main inlet volume flow rate and each of the sheath flow volume flow rates of (1) 25.0 μL/hr and 50.0 μL/hr, (2) 12.5 μL/hr and 25.0 μL/hr with two different acoustic powers of (i) 16.3 mW and (ii) 65 mW.

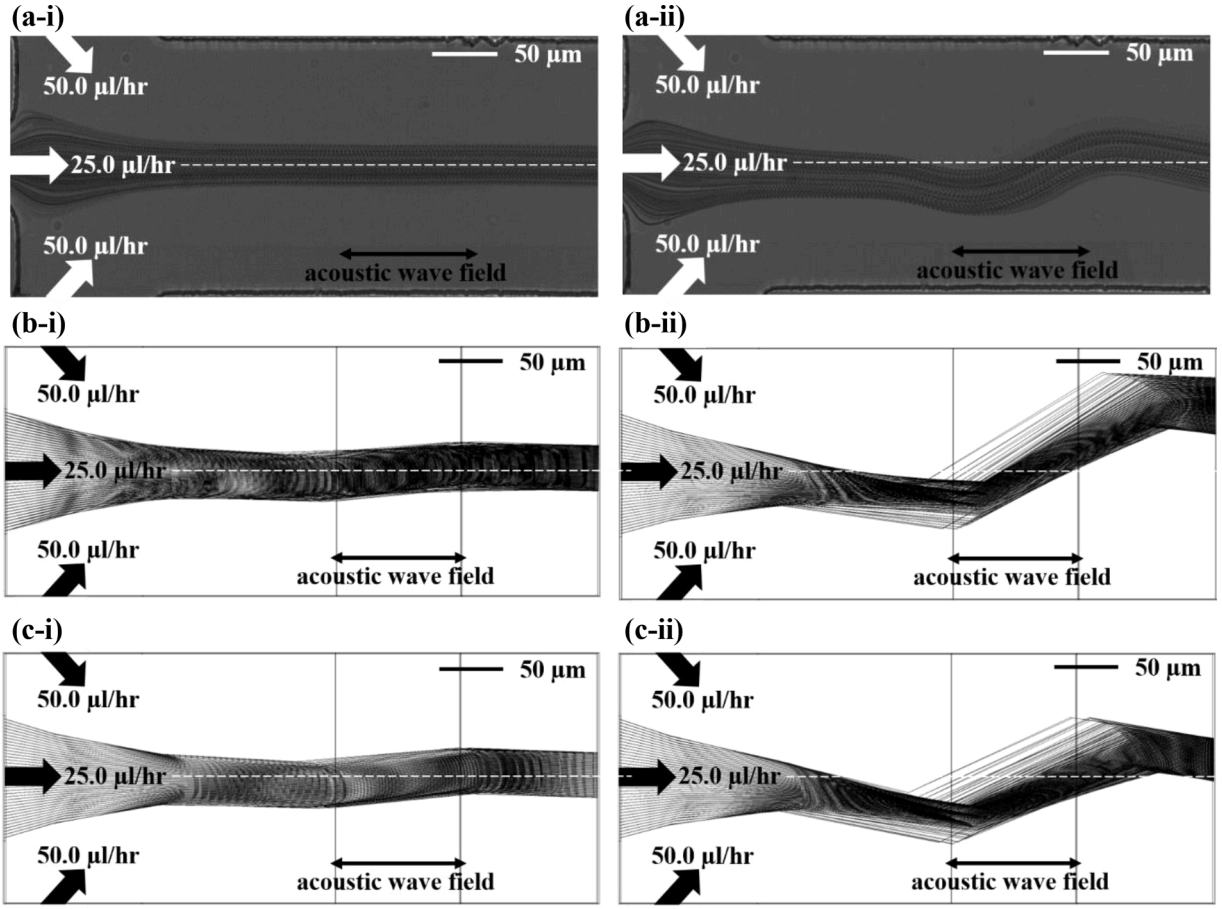

Fig. 9. Flow field results of (a) experimental, (b) computational with the first approach and (c) computational with the second approach for main inlet volume flow rate and each of the sheath flow volume flow rates of 25.0 μL/hr and 50.0 μL/hr with two different acoustic powers of (i) 16.3 mW and (ii) 65 mW.

Using acoustic steaming for droplet sorting

Acoustic streaming is used to sort droplets into the upper outlet while without acoustic streaming the droplets flow into the lower outlet. The experimental and the first approach computational results for droplet trajectories is shown in Fig. 10. The results presented are for acoustic power of 200 mW and a pulse width of 0.3 ms, main inlet volume flow rate of 50.0 μl/hr, upper sheath flow volume flow rate of 55.0 μl/hr and lower sheath flow volume flow rate of 45.0 μl/hr.

The droplet trajectories from both experiment and simulation (Figs. 10(a) and 10(b)) are in good agreements. The volume flow rates of the sheath flows are used that without acoustics the droplets flow into the lower outlet. Switching the SAW device on pushes the droplets along the wave's propagation direction and deflects the droplets into the upper outlet. The graphs for the droplets' velocity magnitude as well as velocity components in x- and z-directions along the length of the microchannel are shown in Fig. 10(c). In the presence of the acoustic field the droplets' velocity increases and as it exits the TSAW region the droplets' velocity decreases to match the flow velocity.

Conclusions

In this paper, effects of acoustic streaming caused by TSAW on fluid and microparticles in a microchannel flow is investigated using numerical simulations with two different approaches. In the first approach, the whole acoustic field is simulated and coupled to the flow field to obtain the results. Whereas for the second approach the effect of acoustic streaming on the flow field was simulated using

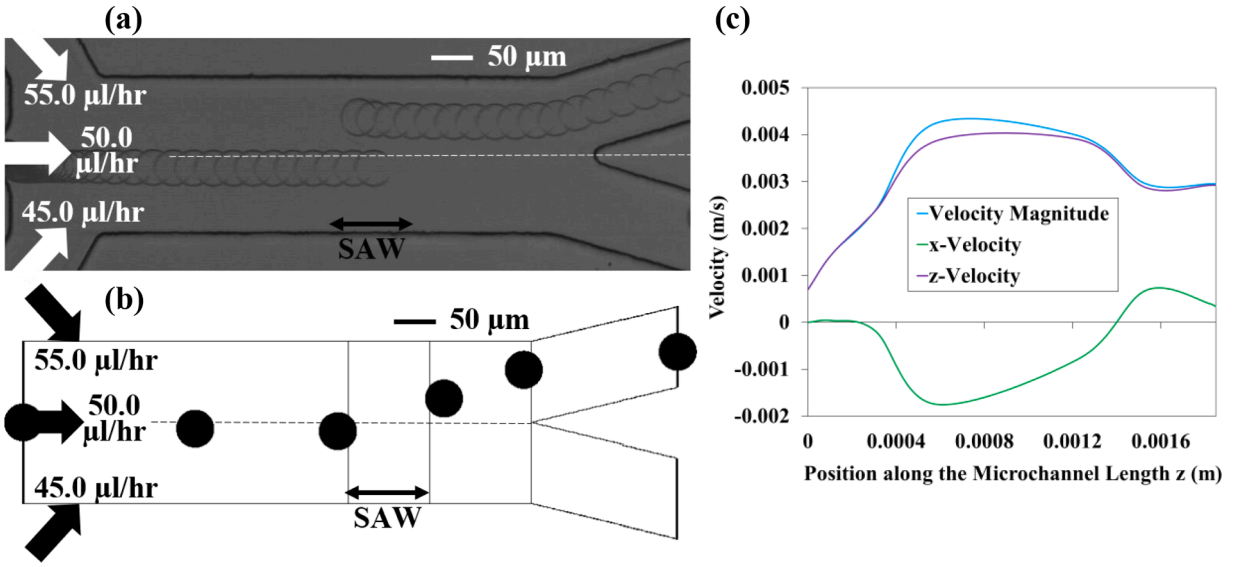

Fig. 10. Droplet trajectories from (a) experimental and (b) computational results and (c) velocity magnitude and components along the z-direction (length) of the microchannel and for main inlet volume flow rate of 50.0 µl/hr, upper sheath flow volume flow rate of 55.0 µl/hr and lower sheath flow volume flow rate of 45.0 µl/hr with acoustic powers of 200 mW and a pulse width of 0.3 ms.

the velocity of a one-dimensional attenuating TSAW in the acoustic streaming force formula. In this approach, the acoustic streaming force is calculated without using the density and velocity caused by the acoustic field.

For this study two main cases are considered. The first case investigates the acoustic streaming effect on the fluid flow inside a microchannel with different inlet and sheath flow rates as well as different acoustic powers with the two different approaches of modelling the acoustic effects. The second case studies the effect of acoustic streaming on the microparticles' movement inside a microchannel with different acoustic powers. For both the cases the computational results are comparable with and verified by experimental data. In the first approach, the acoustic field induced by the TSAW is modelled, and the acoustic streaming force is calculated using the first order density and velocity caused by the acoustic filed. Therfore, this approach predicts the acoustofluidic system more accurately. The second approach models the acoustic streaming effect in a microchannel with its height considerably smaller than its width, by substituing the velocity of a one-dimensional attenuating TSAW in the acoustic streaming force formula without using the density and velocity fields caused by the acoustic field. This aproach is more efficient in terms of computational cost and time while still presenting results with a reasonable accuracy.

The first approch calculates the in-plane velocity components (x-velocity and z-velocity) in the TSAW field more accuratly compared to the second approach, as the second approach underestimates the maximum/minimum value of z-velocity by 14% and overestimates the maximum value of x-velocity by 9%. Thus the velocity magnitude in xz-plane is calculated more accuratly using the first approach compared to the second approach. The out-of-plane velocity component (y-velocity) in the TSAW field calculated by the first approach is 25 times larger than the value given by the second approach. This combined with the differences between the velocity magnitudes in xz-plane calculated by the first and second approaches, results in the total velocity value to be 6 times larger in the SAW field for the first approach compared to the second approach.

Simulation of acoustofluidic setups provides detailed information of the pressure and velocity fields with and without microparticles. It presents the properties of the fluid flow and microparticles under the effect of SAW in a cost and time effective manner which are sometimes hard or even impossible to obtain through experimental work.

Declaration of Competing Interest

The authors declare no conflict of interest.

Acknowledgements

This work was financially supported by the UK Engineering and Physical Sciences Research Council (EPSRC) grants (EP/P018998/1) and (EP/P018882/1), and Special Interests Group of Acoustofluidics under the EPSRC-funded UK Fluidic Network (EP/N032861/1).

References

Batchelor, G. K. (2000). *An Introduction to fluid dynamics (Cambridge Mathematical Library)*. Cambridge: Cambridge University Press.

Beebe, D. J., Mensing, G. A., & Walker, G. M. (2002). Physics and applications of microfluidics in biology. *Annual Review of Biomedical Engineering, 4*(1), 261–286. https://doi.org/10.1146/annurev.bioeng.4.112601.125916

Chen, X., Toh, K., Chai, J., & Yang, C. (2004). Developing pressure-driven liquid flow in microchannels under the electrokinetic effect. *International journal of engineering science, 42*(5-6), 609–622.

Particle tracing module user's guide. (2018). COMSOL, 5.4 ed.

Collins, D. J., et al. (2017). Selective particle and cell capture in a continuous flow using micro-vortex acoustic streaming. *Lab on a chip, 17*(10), 1769–1777. https://doi.org/10.1039/c7lc00215g

Collins, D. J., Ma, Z., Han, J., & Ai, Y. (2017). Continuous micro-vortex-based nanoparticle manipulation via focused surface acoustic waves. *Lab on a chip, 17*(1), 91–103. https://doi.org/10.1039/C6LC01142J

Crowe, C. T. (2005). *Multiphase flow handbook*. CRC press.

Crowe, C. T., Schwarzkopf, J. D., Sommerfeld, M., & Tsuji, Y. (2011). *Multiphase flows with droplets and particles*. CRC press.

Destgeer, G., Im, S., Hang Ha, B., Ho Jung, J, Ansari, M. Ahmad, & Sung, H. Jin (2014). Adjustable, rapidly switching microfluidic gradient generation using focused travelling surface acoustic waves. *Applied Physics Letters, 104*(2), Article 023506. https://doi.org/10.1063/1.4862322

Devendran, C., Albrecht, T., Brenker, J., Alan, T., & Neild, A. (2016). The importance of travelling wave components in standing surface acoustic wave (SSAW) systems. *Lab on a chip, 16*(19), 3756–3766. https://doi.org/10.1039/C6LC00798H

Ding, X., et al. (2013). Surface acoustic wave microfluidics. *Lab on a chip, 13*(18), 3626–3649. https://doi.org/10.1039/C3LC50361E, 10.1039/C3LC50361E.

Doinikov, A. A. (1994). Acoustic radiation pressure on a rigid sphere in a viscous fluid. *Proc. R. Soc. Lond. A, 447*, 447–466. https://doi.org/10.1098/rspa.1994.0150, 1931.

Doinikov, A. A. (1994). Acoustic radiation pressure on a compressible sphere in a viscous fluid. *Journal of Fluid Mechanics, 267*, 1–22. https://doi.org/10.1017/S0022112094001096

Doinikov, A. A. (2003). Acoustic radiation forces: classical theory and recent advances. *Recent Res Devel Acoustics, 1*, 39–67.

Franke, T., Braunmuller, S., Schmid, L., Wixforth, A., & Weitz, D. A. (2010). Surface acoustic wave actuated cell sorting (SAWACS). *Lab on a chip, 10*(6), 789–794. https://doi.org/10.1039/b915522h

Franke, T., Abate, A. R., Weitz, D. A., & Wixforth, A. (2009). Surface acoustic wave (SAW) directed droplet flow in microfluidics for PDMS devices. *Lab on a chip, 9*(18), 2625–2627. https://doi.org/10.1039/B906819H, 10.1039/B906819H.

Friend, J., & Yeo, L. Y. (2011). Microscale acoustofluidics: Microfluidics driven via acoustics and ultrasonics. *Reviews of Modern Physics, 83*(2), 647–704. https://doi.org/10.1103/RevModPhys.83.647, 06/20/2011.

Fu, Y. Q., et al. (2017). Advances in piezoelectric thin films for acoustic biosensors, acoustofluidics and lab-on-chip applications. *Progress in Materials Science, 89*, 31–91. https://doi.org/10.1016/j.pmatsci.2017.04.006

Gorkov, L. P. (1962). On the forces acting on a small particle in an acoustical field in an ideal fluid. *Soviet Physics - Doklady, 6*, 773–775.

Huang, T. J. (2019). Acoustofluidics: Merging acoustics and microfluidics for biomedical applications. *The Journal of the Acoustical Society of America, 145*(3). https://doi.org/10.1121/1.5101531, 2019/03/01 1786–1786.

King, L. V. (1934). On The Acoustic radiation pressure on spheres. *Proceedings of the Royal Society of London. Series A-Mathematical and Physical Sciences, 147*(861), 212–240. https://doi.org/10.1098/rspa.1934.0215

Li, P., & Huang, T. J. (2018). Applications of acoustofluidics in bioanalytical chemistry. *Analytical chemistry, 91*(1), 757–767. https://doi.org/10.1021/acs.analchem.8b03786

Lighthill, J. (1978). Acoustic streaming. *Journal of sound and vibration, 61*(3), 391–418. https://doi.org/10.1007/s001620050068

Liu, S., et al. (2017). Investigation into the effect of acoustic radiation force and acoustic streaming on particle patterning in acoustic standing wave fields. *Sensors (Basel, Switzerland), 17*(7), 1664. https://doi.org/10.3390/s17071664

Nilsson, A., Petersson, F., Jonsson, H., & Laurell, T. (2004). Acoustic control of suspended particles in micro fluidic chips. *(in eng), Lab on a chip, 4*(2), 131–135. https://doi.org/10.1039/b313493h

Nyborg, W. L. (1953). Acoustic streaming due to attenuated plane waves. *The journal of the acoustical society of America, 25*(1), 68–75. https://doi.org/10.1121/1.1907010

Rambach, R. W., Linder, K., Heymann, M., & Franke, T. (2017). Droplet trapping and fast acoustic release in a multi-height device with steady-state flow. *Lab on a chip, 17*(20), 3422–3430.

Sackmann, E. K., Fulton, A. L., & Beebe, D. J. (2014). The present and future role of microfluidics in biomedical research. *(in eng), Nature, 507*(7491), 181–189. https://doi.org/10.1038/nature13118

Sadhal, S. S. (2012). Acoustofluidics 13: Analysis of acoustic streaming by perturbation methods. *Lab on a chip, 12*(13), 2292–2300. https://doi.org/10.1039/C2LC40202E, 10.1039/C2LC40202E.

Schmid, L., Weitz, D. A., & Franke, T. (2014). Sorting drops and cells with acoustics: acoustic microfluidic fluorescence-activated cell sorter. *Lab on a chip, 14*(19), 3710–3718. https://doi.org/10.1039/c4lc00588k

Settnes, M., & Bruus, H. (2012). Forces acting on a small particle in an acoustical field in a viscous fluid. *Physical Review E, 85*(1), Article 016327. https://doi.org/10.1103/PhysRevE.85.016327

Shiokawa, S., Matsui, Y., & Ueda, T. (1990). Study on SAW streaming and its application to fluid devices. *Japanese journal of applied physics, 29*(S1), 137.

Singh, A. K., Kumar, S., & Chattopadhyay, A. (2015). Love-type wave propagation in a piezoelectric structure with irregularity. *International Journal of Engineering Science, 89*, 35–60.

Sivanantha, N., et al. (2014). Characterization of adhesive properties of red blood cells using surface acoustic wave induced flows for rapid diagnostics. *Applied Physics Letters, 105*(10), Article 103704.

Skowronek, V., Rambach, R. W., & Franke, T. (2015). Surface acoustic wave controlled integrated band-pass filter. *Microfluidics and Nanofluidics, 19*(2), 335–341.

Thielicke, W., & Stamhuis, E. (2014). PIVlab–towards user-friendly, affordable and accurate digital particle image velocimetry in MATLAB. *Journal of open research software, 2*(1).

Thielicke, W., & Stamhuis, E. J. (2018). The effects of wing twist in slow-speed flapping flight of birds: trading brute force against efficiency. *Bioinspiration & biomimetics, 13*(5), Article 056015.

Thielicke, W. (2014). *The Flapping flight of birds: analysis and application*. University of Groningen.

Walls, P. L., & Abedian, B. (2014). Bivelocity gas dynamics of micro-channel couette flow. *International Journal of Engineering Science, 79*, 21–29.

Wang, K., et al. (2017). Sorting of tumour cells in a microfluidic device by multi-stage surface acoustic waves. *Sensors and Actuators B Chemical, 258*. https://doi.org/10.1016/j.snb.2017.12.013

Whitesides, G. M. (2006). The origins and the future of microfluidics. *Nature, 442*, 368. https://doi.org/10.1038/nature05058

Yosioka, K., & Kawasima, Y. (1955). Acoustic radiation pressure on a compressible sphere. *Acta Acustica united with Acustica, 5*(3), 167–173.